Five year (2004–2009) observations of upper tropospheric water vapor and cloud ice from MLS and comparisons with GEOS-5 analyses

Jonathan H. Jiang,[1] Hui Su,[1] Steven Pawson,[2] Hui-Chun Liu,[2] William G. Read,[1] Joe W. Waters,[1,3] Michelle L. Santee,[1] Dong L. Wu,[1] Michael J. Schwartz,[1] Nathaniel J. Livesey,[1] Alyn Lambert,[1] Ryan A. Fuller,[1] and Jae N. Lee[1]

Received 25 September 2009; revised 3 March 2010; accepted 12 March 2010; published 3 August 2010.

[1] This paper gives an overview of August 2004 through February 2010 upper tropospheric (UT) water vapor (H_2O) and ice water content (IWC) from the Aura Microwave Limb Sounder (MLS) and comparisons with outputs from the NASA Goddard Earth Observing System Version 5 (GEOS-5) data assimilation system. Both MLS and GEOS-5 show that high values of H_2O and IWC at 215 to 147 hPa are associated with areas of deep convection. They exhibit good (within ~15%) agreement in IWC at these altitudes, but GEOS-5 H_2O is ~50% (215 hPa) to ~30% (147 hPa) larger than MLS values, possibly due to higher temperatures in the data assimilation system at these altitudes. A seasonally migrating band of tropical deep convection is clearly evident in both the MLS and GEOS-5 UT H_2O and IWC, but GEOS-5 produces a weaker intertropical convergence zone than MLS. MLS and GEOS-5 both show spatial anticorrelation between IWC and H_2O at 100 hPa, where low H_2O is associated with low temperatures in regions of tropical convection. At 100 hPa, GEOS-5 produces 50% less IWC and 15% less H_2O in the tropics, and ~20% more H_2O in the extratropics, than does MLS. Behavior of the 100 hPa H_2O is consistent with it being controlled by temperature. The seasonal cycle in the vertical transport of tropical mean H_2O from ~147 hPa to ~10 hPa appears much stronger in MLS than in GEOS-5. The UT IWC and H_2O interannual variations, from both MLS and GEOS-5, show clear imprints of the El Niño–Southern Oscillation.

Citation: Jiang, J. H., et al. (2010), Five year (2004–2009) observations of upper tropospheric water vapor and cloud ice from MLS and comparisons with GEOS-5 analyses, *J. Geophys. Res.*, *115*, D15103, doi:10.1029/2009JD013256.

1. Introduction

[2] Upper-tropospheric (UT) water vapor (H_2O) and clouds play important roles in regulating Earth's climate, producing feedbacks in response to increasing greenhouse gases. H_2O is the primary natural atmospheric greenhouse gas, trapping some of the outgoing longwave radiation (OLR) that would otherwise be emitted to space. The increase of UT H_2O with sea surface temperature (SST) provides a strong positive feedback in response to surface temperature increases that can be caused by increasing anthropogenic greenhouse gases [e.g., *Held and Soden*, 2000; *Su et al.*, 2006a]. *Udelhofen and Hartmann* [1995] showed that OLR is most sensitive to UT relative humidity changes above 400 hPa. Climate models indicate that UT specific humidity or H_2O could increase ~200% by the end of the 21st century, compared to a ~20% increase in lower tropospheric H_2O [*Soden et al.*, 2005]. This UT amplification underscores the importance of monitoring and quantifying UT H_2O variability.

[3] Clouds in the UT tend to have a net warming effect, as their cold tops result in low OLR [*Stephens*, 1990; *Su et al.*, 2009]. The occurrence of UT clouds is closely related to UT humidity [*Udelhofen and Hartmann*, 1995; *Soden and Fu*, 1995; *Su et al.*, 2006a]. The variation of UT cloud amount with SST and the resulting potential climate feedback have been a subject of debate [*Lindzen et al.*, 2001; *Lin et al.*, 2002; *Hartmann and Michelsen*, 2002; *Su et al.*, 2009]. The UT cloud radiative heating also influences transport from the troposphere to the stratosphere [e.g. *Corti et al.*, 2006; *Hartmann et al.*, 2001].

[4] The Microwave Limb Sounder (MLS) on board the Aura satellite, launched on July 15, 2004, provides simultaneous global measurements of UT H_2O, cloud ice water content (IWC), temperature (T), and several trace gases [*Waters et al.*, 2006]. *Li et al.* [2005, 2007] compared Aura MLS IWC measurements with European Centre for

[1]Jet Propulsion Laboratory, California Institute of Technology, Pasadena, California, USA.
[2]Global Modeling and Assimilation Office, NASA Goddard Space Flight Center, Greenbelt, Maryland, USA.
[3]Retired.

Copyright 2010 by the American Geophysical Union.
0148-0227/10/2009JD013256

Medium-range Weather Forecast (ECMWF) analyses and forecasts, and with other state-of-the-art climate model simulations, and found differences as large as a factor of 10 between models and observations. These helped promote modifications to the ECMWF model cloud microphysics that resulted in significant improvement [*Waliser et al.*, 2009]. *Su et al.* [2006b] found differences between models and observations of up to a factor of four in slopes of the fitted linear relationships among UT H_2O, IWC, and SST. *Read et al.* [2008], using MLS H_2O and CO measurements, estimated the relative contributions of convection, "freeze-drying" (a dehydration process by which liquid or ice clouds are formed when vapor saturation is reached and the condensates sediment out) and extra-tropical mixing on the amount of H_2O entering the stratosphere. *Read et al.* [2008] shows that H_2O mixing ratios in the tropical tropopause layer (TTL) are mainly controlled by large scale freeze-drying.

[5] This paper presents an overview of the global distributions and temporal variations for UT IWC and H_2O as seen by MLS from August 2004 through February 2010 (the period for which data are currently available), spatial correlations with deep convection and temperature, and comparisons with output from the Goddard Earth Observing System Version 5 (GEOS-5) data assimilation system. Section 2 describes the datasets, Section 3 presents spatial distributions, and Section 4 presents temporal variations. Section 5 focuses on the UT response to the El Niño-Southern Oscillation (ENSO). Section 6 gives conclusions and discussion.

2. Data

2.1. Aura MLS UT Water Vapor, Cloud, and Temperature Measurements

[6] We use MLS Version 2.2 (V2.2) Level 2 [*Livesey et al.*, 2007] H_2O, IWC and T datasets, whose validations are described by *Read et al.* [2007], *Wu et al.* [2008], and *Schwartz et al.* [2008], respectively. MLS measures ~3500 vertical profiles per day along a sun-synchronous suborbital track having equatorial crossings at 1:40 PM and 1:40 AM local solar times. The Level 2 data are produced on pressure surfaces (12 surfaces per decade) from 316 to 0.1 hPa, with IWC having a limited useful range of 215 to 83 hPa. These data have a vertical resolution of ~3–4 km, and horizontal resolutions of ~7 km across-track and ~200–300 km along-track. Estimated measurement accuracies are 20% for H_2O, 2 K for temperature, and a factor of two for IWC.

[7] The MLS H_2O and temperature are two independent products. The uncertainty in temperature retrieval does not generally affect the H_2O retrieval [*Read et al.*, 2007]. The uncertainty of MLS IWC measurement due to uncertainties in particle size distribution (PSD) and habits is reported by *Wu et al.* [2008]. The PSD-related uncertainty in MLS V2.2 IWC retrieval is estimated to be about 100% and the habit-related uncertainty is less than 20%. *Schwartz et al.* [2008] showed that MLS V2.2 temperature has a low bias of ~2 K at 215 hPa and of ~0.5 K at 147 hPa with respect to coincident radiosondes, GPS occultation retrievals, and analysis profiles. Possible sources of bias in MLS temperature profiles include small effects of radiometer nonlinearity, standing waves in optics and slight misplacement of band pass filters.

[8] MLS measurements are generally not degraded by the presence of clouds and aerosols, whose particle sizes are typically much smaller than the measurement wavelengths. Very thick clouds (IWC > ~50 mg/m^3) can degrade the temperature and some species measurements [*Wu et al.*, 2008], but the retrieval algorithms [*Livesey et al.*, 2006] flag such measurements and they are not used here. See *Wu and Jiang* [2004] for details on the identification and quantification of cloud-affected radiances and the IWC retrieval.

2.2. GEOS-5 Meteorological Products

[9] Meteorological datasets produced by the GEOS Versions 5.1.0 and 5.2.0 data assimilation systems are used in this study. *Rienecker et al.* [2008] described the meteorological analysis, which uses a three-dimensional variational (3D-Var) approach [*Sasaki*, 1970]. GEOS-5.1.0 was run in near-real time between 17 October 2007 and 14 August 2008; it was also used to retroactively analyze the period from October 2003, before the Aura launch, until October 2007. GEOS-5.1.0 was replaced by GEOS-5.2.0 on 14 August 2008. Both versions, collectively referred to as GEOS-5, produce analyses, forecasts and assimilated fields on a 72-layer grid, extending from the surface to 0.01 hPa, with a 0.5° × 0.67° latitude-longitude resolution. Vertical resolution is ~1.5 km in the UT. Differences between the two versions of GEOS-5 will be mentioned as necessary in the presentation of results.

[10] The GEOS-5 analyses are "snapshots" of the atmospheric state produced four times daily (at 00Z, 06Z, 12Z, and 18Z) using optimal combinations of model forecasts and many observations [*Rienecker et al.*, 2008] via the Grid-point Statistical Interpolation (GSI) technique of *Wu et al.* [2002]. The assimilated fields are continuous time series produced using the GEOS-5 atmospheric general circulation model (AGCM), in which an additional forcing term is added to the momentum, thermodynamic, moisture and ozone equations, following *Bloom et al.* [1996]. This "incremental analysis update" (IAU) forcing is computed from the difference between analysis and AGCM forecast at the analysis times, then added as a forcing tendency that remains constant in six-hour segments that straddle the analysis times. The assimilated data are these AGCM fields that are constrained by the analyses and contain all information derived from the model, such as cloud and radiation fields, in addition to the analyzed variables [*Rienecker et al.*, 2008].

[11] The importance of transport to the moisture budget and the fact that all clouds in the GEOS-5 assimilations depend strongly on the AGCM require that some details of the model be mentioned for understanding the products. The GEOS-5 AGCM is coded flexibly, but used in particular configurations (spatial resolution and physical parameter settings) in each version of the assimilation system. Adiabatic transport is computed using the "finite-volume dynamical core" [*Lin*, 2004] with a quasi-Lagrangian vertical coordinate, followed by remapping to the standard 72-layer hybrid grid on which physical tendencies are computed every 30 minutes. The model includes prognostic equations for large-scale gases, liquid (condensate) and ice (anvil-type)

water, with consideration of sub-grid convective contributions to the large-scale liquid and ice phases. Convection is computed using an adaptation of the Relaxed Arakawa-Schubert (RAS) convection code [*Moorthi and Suarez*, 1992], with modifications based on work by *Sud and Walker* [1999] as described by *Bacmeister et al.* [2006]. RAS considers a sequence of detraining convective plumes extending between cloud base (set as a fixed layer in GEOS-5, but inherently adaptable in RAS) and each layer below the tropopause region (close to 100 hPa); each plume produces detraining mass and cloud condensate at each layer and also modifies the environmental meteorological (temperature, moisture, wind) profiles felt by the next plume. The large-scale cloud condensate scheme, based on probability distribution functions (PDFs) of the moisture field assumed inside a grid box, incorporates changes to condensate and anvil clouds obtained from RAS, then computes new sources for the anvil cloud (freezing of existing condensate) and new partitioning of condensate, before computing loss due to evaporation, auto-conversion of liquid or mixed-phase condensate, sedimentation of frozen condensate, and accretion of condensate by falling precipitation. Details of these processes are given by *Rienecker et al.* [2008] (http://gmao.gsfc.nasa.gov/pubs/docs/GEOS5_104606-Vol27.pdf).

[12] Atmospheric moisture in GEOS-5 is analyzed in the form of relative humidity along with other analysis variables including the stream function, the unbalanced part of velocity potential, temperature, surface pressure, ozone, cloud liquid and ice water, and regression coefficients for radiance bias correction. The optimal analysis is obtained by finding the best fit to the six-hourly forecast field and observations while minimizing the cost function. Various types of observations such as radiosondes and radiances from the Microwave Humidity Sounder (MHS), the Special Sensor Microwave/Imager (SSM/I) and the Atmospheric Infrared Sounder (AIRS) provide information to constrain the moisture fields. AIRS, in particular, gives information on vertical structure for atmospheric temperature and moisture due to its sounding capability. A total of 152 spectral channels from AIRS are currently assimilated in GEOS-5; these are selected from the 281-channel "NWP subset" of AIRS radiance measurements. While most of the AIRS channels are subject to water vapor absorption, it is most significant in the infrared portion of the spectrum from 6.20 μm to 8.22 μm. At present, 49 of the water vapor channels from this band are being assimilated. These water vapor absorption channels peak at different pressure levels in the troposphere, providing information on the vertical distribution of moisture for the analysis. The observation error covariance matrix for radiance data is assumed to be diagonal, i.e., possible inter-channel correlations are neglected. The error values assigned to the water vapor channels are larger than those assigned to temperature channels in order to account for the possibility of inter-channel error correlations, the effects of undetected residual cloud, and the non-linear nature of the moisture channels that is not accounted for in the formulation of Jacobians in the 3D-Var analysis. However, AIRS water vapor data degrade at altitudes above 200 hPa [*Fetzer et al.*, 2008] and thus do not provide information in the upper troposphere with pressure < 200 hPa and in stratosphere.

[13] In the GEOS-5 model, the stratospheric water vapor is relaxed to zonal-mean (latitude-height) monthly mean values that come from a zonal-mean model simulation with boundary conditions for the year 2000. This includes a weak annual cycle of about 3.5–4 ppmv in the tropical lower stratosphere, which explains a weak tape recorder signal there. It also includes a height-dependent increase that is a proxy for methane oxidation at higher levels. Relaxation time to these zonal-mean values is a few days.

[14] Although GEOS-5 does not allow relative humidity to exceed 100% in regards to its modeling of cloud physics and parameterization, super-saturation can still occur in GEOS-5 output. This is because temperature and moisture values can be affected by physics and chemistry that are modeled in the AGCM after the cloud processes are modeled.

[15] For comparison with MLS, the GEOS-5 data are interpolated onto the MLS measurement locations in both space and time. Previous studies [e.g., *Li et al.*, 2007; *Su et al.*, 2006b] have shown that such interpolation is particularly important because of potential artifacts that arise from incomplete sampling of the diurnal cycle by polar-orbiting satellites. For horizontal sampling, GEOS-5 data are collocated with MLS data by averaging the data in boxes of 3° along the track and 1° across the track centered on the MLS measurement locations (approximately matching the MLS footprints). Vertically, the respective MLS averaging kernels [*Read et al.*, 2007; *Schwartz et al.*, 2008] are applied to the GEOS-5 H_2O mixing ratio and temperature products. The GEOS-5 IWC data are averaged in vertical boxes of ~3.5 km centered on MLS data points to mimic the MLS IWC vertical resolution [*Wu et al.*, 2008].

3. Global Distribution of UT H_2O and IWC

3.1. Annual Mean Maps

[16] Figure 1 shows five-year mean (January 2005 to December 2009) annual IWC, H_2O and T maps at three pressure levels (100, 147, and 215 hPa), from both MLS observations and GEOS-5 analyses. Contours enclosing GEOS-5 OLR of 240 Wm^{-2} or less (indicating regions of deep convection), and potential vorticity contours of 3.5×10^{-6} Km^2 $kg^{-1}sec^{-1}$ (PV3.5, indicating the poleward edge of dynamical tropopause), are superimposed. Both MLS and GEOS-5 data show that at 215 and 147 hPa, large IWC and H_2O and low OLR are collocated in the tropical western Pacific, west central Africa and northern South America. The PV3.5 contour generally encloses the large IWC and H_2O values, supporting the notion that it generally marks the boundary between tropospheric and stratospheric air [e.g., *Danielsen*, 1968; *Highwood et al.*, 2000; *Schoeberl*, 2004]. Poleward of the PV3.5 contours, there are relatively few clouds and H_2O concentrations are low. The PV3.5 contours also enclose warm regions at 215 hPa, related to latent heat release from tropical convection, and low T values at 147 and 100 hPa, where adiabatic cooling in upwelling dominates as convective influence extends up to the cold tropopause. Higher stratospheric T values are found poleward of the PV3.5 contour. At 100 hPa, both MLS and GEOS-5 have minimum H_2O over the Western Pacific, extending somewhat to the east of the lowest OLR, but coincident with minimum T. The convective regions over

equatorial South America and Africa are warmer and moister at 100 hPa than that over the Western Pacific, consistent with the premise that T controls humidity near the tropical tropopause [*Holton and Gettelman*, 2001; *Read et al.*, 2004], although convective dehydration may also play a role [*Sherwood and Dessler*, 2001]. Using a 2-D TTL model, *Read et al.* [2008] suggested that "freeze-drying" associated with large-scale advection dominates the H_2O

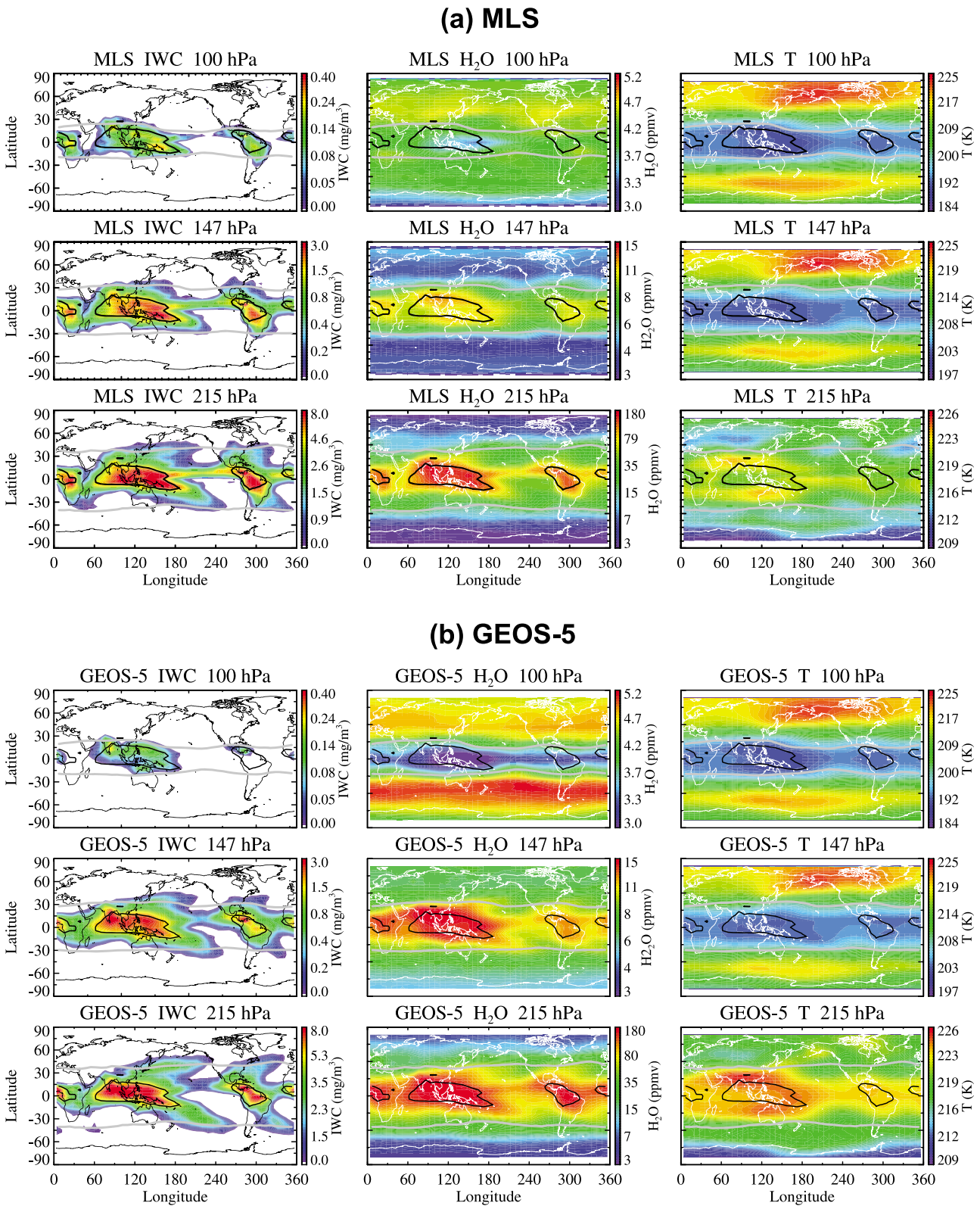

Figure 1

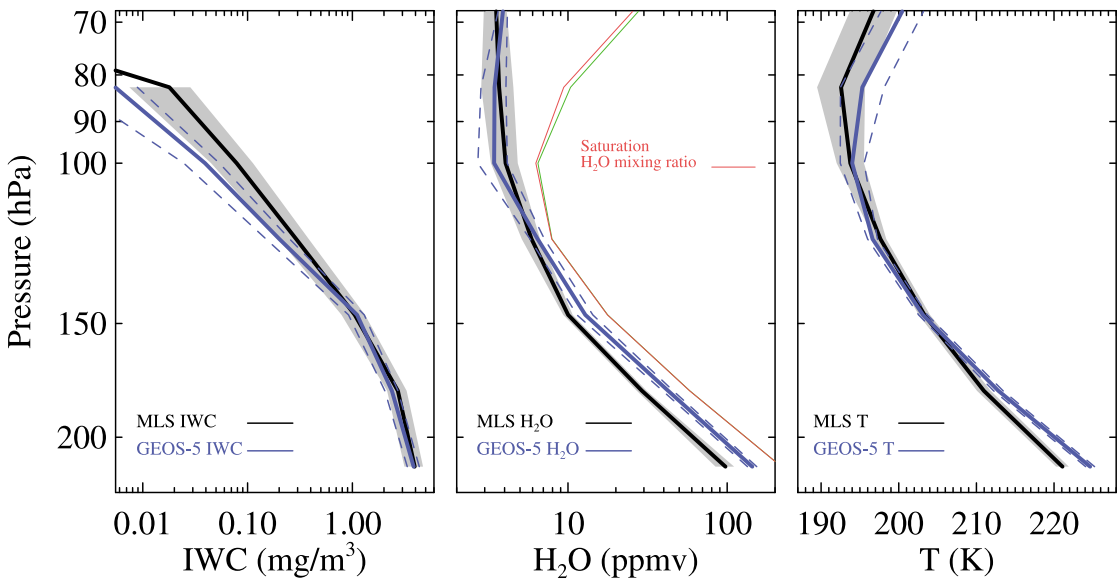

Figure 2. Tropical (15°S–15°N) mean IWC, H_2O and T profiles from both MLS (black) and GEOS-5 (blue). The profiles are averages of daily mean tropical profiles from January 2005 to December 2009. The standard deviations of daily profiles for MLS (gray-shade) and GEOS-5 (blue-dashed) are also shown, as well as the saturation specific humidity profile (green) computed using the GEOS-5 temperature.

entry value into the stratosphere, while convection and ice re-evaporation have a clearer imprint on water vapor isotopes in the TTL than on H_2O.

[17] GEOS-5 IWC and H_2O at 215 hPa are quite similar to MLS fields both in morphology and in magnitude, although GEOS-5 is moister than MLS at this level. GEOS-5 at 147 hPa has less IWC and more H_2O than MLS. This might be due to too much sublimation and/or too little condensation in the model's microphysics. GEOS-5 at 100 hPa has smaller values of IWC and is drier in the tropics and wetter in the extra-tropics than MLS. The stronger latitudinal gradient of 100 hPa H_2O in GEOS-5 may indicate some deficiencies in its representation of mass transport from the troposphere (tropics) to the stratosphere (extra-tropics). GEOS-5 is on average warmer than MLS in the tropics by ~3 K at 215 hPa and ~1 K at 147 hPa, which is not unexpected due to the known MLS low biases in cloudy regions (~2 K at 215 hPa and ~0.5 K at 147 hPa [*Schwartz et al.*, 2008]). MLS and GEOS-5 tropical 100 hPa temperatures agree to within ~0.5 K.

[18] Figure 2 shows the five-year (January 2005 to December 2009) tropical (15°S–15°N) mean profiles of IWC, H_2O and T from both MLS and GEOS-5, along with their daily standard deviations from the five-year mean. The GEOS-5 IWC profile agrees within 12% with MLS at 215 hPa to 147 hPa but becomes 30%, 50% and 70% smaller than the MLS IWC at 121 hPa, 100 hPa and 83 hPa, respectively. Although these are all within the estimated (factor of 2) uncertainty of MLS measurements, the smaller GEOS-5 IWC amounts above 147 hPa suggest that convection in the model does not extend to sufficiently high altitudes.

[19] The GEOS-5 and MLS differences in tropical H_2O and T appear to have a source other than that for the IWC differences. GEOS-5 H_2O is limited to values corresponding to 100% or less relative humidity, and an overestimate of T could possibly lead to an overestimate of H_2O. Figure 2 shows that, after accounting for the known MLS ~2 K cold bias, GEOS-5 215 and 178 hPa tropical T is still larger than that of MLS by ~1 K, which may contribute to the large H_2O in GEOS-5 at the two levels. However, at altitudes above 121 hPa, GEOS-5 H_2O is smaller than MLS, but the saturation H_2O mixing ratio profile computed using GEOS-5 T is much larger than both MLS and GEOS-5 H_2O, suggesting that temperature bias in GEOS-5 cannot explain the H_2O discrepancy between MLS and GEOS-5 at 121 hPa altitude and above. In summary, GEOS-5 tropical mean 215 hPa H_2O is larger than that of MLS by ~50% and tropical mean 215 hPa T is higher by ~3.5 K, both of which are significant compared to estimated MLS measurement

Figure 1. Annual mean IWC, H_2O and temperature maps at 100, 147 and 215 hPa pressure levels from (a) MLS observations and (b) GEOS-5 analyses. The black contour is the GEOS-5 OLR at 240 Wm^{-2}, and the areas enclosed by the black contours have OLR values less than 240 Wm^{-2}. The lighter grey contour is the GEOS-5 PV3.5. At northern hemisphere, the regions north of the PV3.5 contour have PV values greater than 3.5×10^{-6} $Km^2kg^{-1}sec^{-1}$, while at southern hemisphere, the regions south of PV3.5 contour have PV less than -3.5×10^{-6} $Km^2kg^{-1}sec^{-1}$. The GEOS-5 data are averaged onto 3°×1° boxes centered on MLS measurement locations. MLS averaging kernels are applied to GEOS-5 H_2O and temperature data, and GEOS-5 IWC data are also vertically averaged in 3.5 km boxes centered on MLS data points. Five years of data from January 2005 to December 2009 are used to compute the averages shown in this Figure. Thus the maps are five-year average of "annual means", computed in 8° longitude × 4° latitude grid boxes.

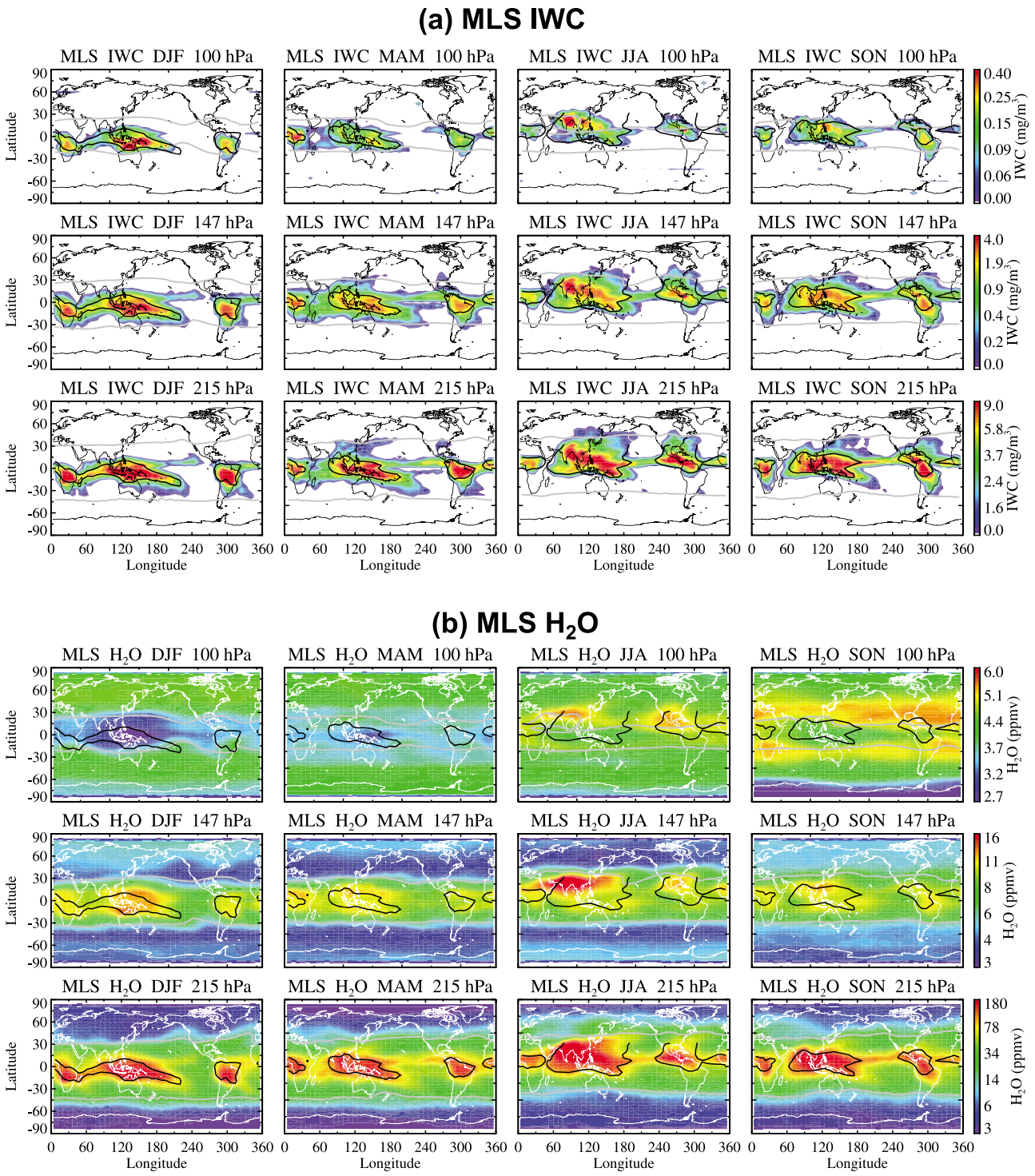

Figure 3. Seasonal mean MLS (a) IWC and (b) H_2O maps at 100, 147 and 215 hPa pressure levels. The black contour is the GEOS-5 OLR at 240 Wm^{-2}. The grey contour is the GEOS-5 PV3.5. Data from December 2004 to October 2009 are used to compute the seasonal averages shown here. Each season includes 3 months from five different years. For example, JJA seasonal map is the average of June–August 2005, June–August 2006, June–August 2007, June–August 2008, and June–August 2009; DJF seasonal map is the average of December 2004–February 2005, December 2005–February 2006, December 2006–February 2007, December 2007–February 2008, and December 2008–February 2009. All the maps are computed in 8° longitude × 4° latitude grid boxes.

uncertainties. GEOS-5 and MLS tropical mean 147 hPa H_2O agree within ~30% (only slightly larger than the estimated 20% MLS measurement uncertainty) and tropical mean 147 hPa T agree to ~0.2 K (within the MLS measurement uncertainty). GEOS-5 and MLS tropical mean 100 hPa H_2O agree to ~15% and T to 0.2 K (both within the MLS measurement uncertainty).

3.2. Seasonal Maps

[20] Figure 3 shows seasonal MLS IWC and H_2O maps at 100, 147 and 215 hPa. The overlaid 240 Wm^{-2} OLR contour generally encloses the highest values of both IWC at all three pressure levels and H_2O at 147 and 215 hPa. High IWC in December to February (DJF) is concentrated south of the Equator in central-south Africa, the Western Pacific and South America. In June–August (JJA), the maximum IWC is distributed over the South Asian monsoon region, while South American convection has shifted northward to Central America. Seasonal variations over the western Pacific are relatively small. The seasonal variation of the ITCZ (Inter-Tropical Convergence Zone) and SPCZ (South Pacific Convergence Zone) is also apparent in MLS IWC.

[21] At 215 hPa, maxima in both IWC (Figure 3a) and H_2O (Figure 3b) are collocated with low OLR, indicating convective moistening of the UT in all seasons. At 147 hPa, the H_2O maxima are over the western Pacific in DJF, and over South Asia in JJA, in both cases slightly north of the strongest convection. Studies using MLS data [e.g., *Fu et al.*, 2006; *Park et al.*, 2007] have shown convectively-lofted H_2O is trapped in the strong anti-cyclone over the Tibetan Plateau during the Asian summer monsoon, where high IWC and H_2O are seen distributed across the tropopause (PV3.5 contour) into the lower stratosphere. At 100 hPa, the minimum H_2O values are found in the cold region over the tropical western Pacific in all four seasons.

[22] Comparing MLS and GEOS-5 maps (shown in auxiliary material Figure S1), there is overall similarity in both IWC and H_2O in terms of seasonal variations, with the differences shown in Figures 1 and 2 also evident in the seasonal maps.[1] However, GEOS-5 shows a much less evident IWC ITCZ feature than MLS, especially in DJF and JJA. This is thought to be due to GEOS-5 underestimating the height of convective penetration in those areas, as mentioned earlier.

[23] Since MLS measurements in the tropics occur in early afternoon and early morning, the impact of the diurnal cycle of deep convection on UT IWC and H_2O is coarsely sampled. Figure 4a shows the 5-year (2005–2009) January and July mean MLS IWC at 215 hPa for day-time (ascending orbits) and night-time (descending orbits). Over the tropical continents (e.g. South America, Africa and South Asia), the mean day-time IWC is about 2 times larger than the night-time IWC. Over the tropical oceans, the day-time IWC is about 50% smaller than the night-time IWC. Comparing with GEOS-5 (Figure 4b) analyses sampled at the same times, the simulated day-night IWC change is much smaller, suggesting that the analyses do not properly represent the diurnal variation of deep convection. The MLS observed UT H_2O diurnal change is within 10%, much smaller than that of IWC, because H_2O is much longer lived and more subject to both horizontal and vertical transport than IWC. We note that the day-night differences shown in Figure 4a do not capture the full amplitude of diurnal changes of clouds and H_2O, as Aura MLS observes two local solar times each day.

4. Time Evolution of UT H_2O and IWC

4.1. Latitude-Time Evolution

[24] Latitude-time sections of daily zonal-mean IWC and H_2O from MLS (Figure 5a) and GEOS-5 (Figure 5b) further illustrate the seasonal evolution from 8 August 2004 to 10 February 2010. The patterns of evolution of 215 and 147 hPa H_2O and IWC, as well as 100 hPa IWC are qualitatively similar, while the 100 hPa H_2O pattern is noticeably different in both MLS and GEOS-5. At 215 and 147 hPa in MLS and GEOS-5, the meridional movements of high IWC and H_2O are in phase and follow the Sun, with highest IWC and H_2O in the northern summer. While the GEOS-5 147 and 215 hPa IWC are in acceptable agreement (within ~15%) with MLS, the GEOS-5 147 and 215 hPa H_2O maxima are larger than MLS by ~30% to 50% throughout the year, as in Figure 1. MLS 100 hPa IWC is confined to a narrow latitudinal band, which shifts seasonally in a similar way to 215 and 147 hPa IWC. The underestimate of 100 hPa IWC in GEOS-5 compared to MLS is clearly a year-round feature. The seasonal cycle in 100 hPa H_2O is very different from that at 147 and 215 hPa. The 100 hPa H_2O is approximately correlated with the annual cycle of temperature, with minima occurring over the Equator in boreal winter and spring. Annual maxima occur more or less simultaneously in both hemispheres (around September), with larger values of 100 hPa H_2O in the northern hemisphere (NH) than in the southern hemisphere (SH). GEOS-5 NH (0°–60°N mean) 100 hPa H_2O values are lower than MLS by ~20%. In the SH (0°–60°S), GEOS-5 shows larger H_2O (~20% larger than MLS) which also persists longer throughout the year than in the NH. The C-shaped latitudinal 100 hPa H_2O maxima in MLS indicate some degree of latitudinal mixing, which is not represented in the GEOS-5. The modeled high H_2O values in the SH are likely due to problems in the model related to relaxation to zonal-mean stratosphere moisture values. We also noted that both the IWC and H_2O fields of GEOS-5 at 215 hPa and 147 hPa have a broader latitudinal extent than those of MLS. Whether this is an indication of the inaccuracy of the regions of convective activity in the model or MLS misses some relatively thin clouds needs further investigation.

4.2. Height-Time Evolution

[25] Figure 6a shows the height-time section of tropical (15°S–15°N) daily mean MLS H_2O anomalies from the tropical mean averaged from 8 August 2004 to 10 February 2010 time period, illustrating the so-called tropical "tape-recorder" signal [*Mote et al.*, 1996] (the imprint of tropical tropopause temperatures, through "freeze-drying", on water vapor entering the stratosphere). There is a clear vertical transport of H_2O from 121 hPa through the stratosphere. H_2O signals imprinted at the bottom of the stratosphere are maintained through the stratosphere for 12 to 18 months as the air rises. The tape recorder is less clear in the upper strato-

[1]Auxiliary materials are available in the HTML. doi:10.1029/2009JD013256.

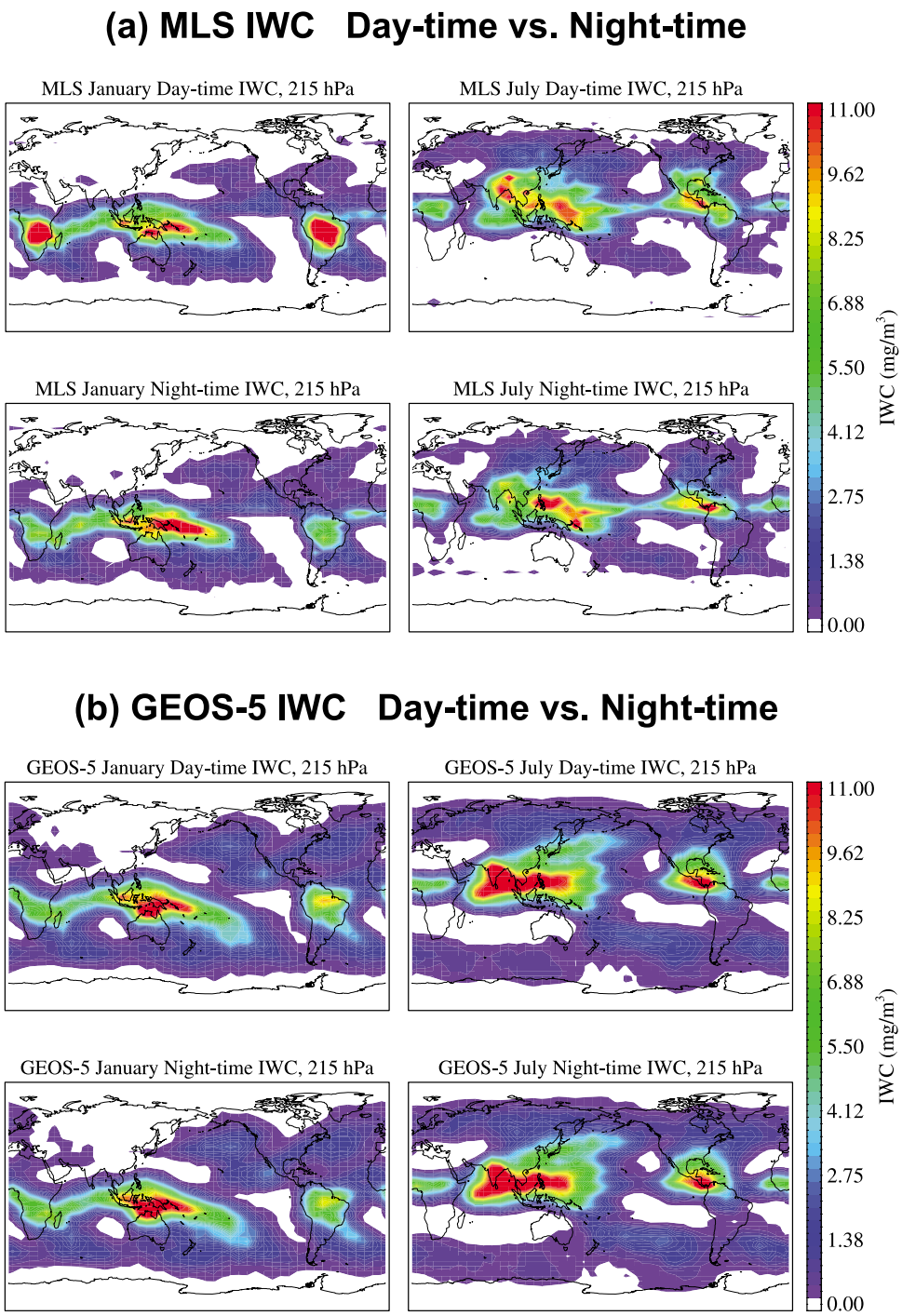

Figure 4. Day-time and night-time maps of five-year (2005–2009) mean January and July IWC from (a) MLS and (b) GEOS-5.

sphere, although the two intense dry phases are especially evident up to ~1 hPa, possibly related to the quasi biennial oscillation (QBO) [e.g., *Baldwin et al.*, 2001]. The seasonal cycle of GEOS-5 tropical H_2O anomalies (Figure 6b) near 100 hPa has a similar magnitude to that of MLS. The amplitude of the GEOS-5 annual cycle at pressures less than 68 hPa decreases more rapidly than that of MLS, although the ascent rates are quite similar. This attenuation of the signal in GEOS-5 arises because of its relaxation of stratospheric moisture to zonal-mean values. Such a tape recorder signal does not appear in the IWC field, since ice is subject to sedimentation, and the warmer stratosphere quickly sublimates ice particles.

4.3. Longitude-Time Evolution

[26] Figure 7 shows the longitude-time section of monthly tropical (15°S–15°N) mean MLS IWC and H_2O anomalies, relative to monthly mean averages for 2005–2009. On inter-

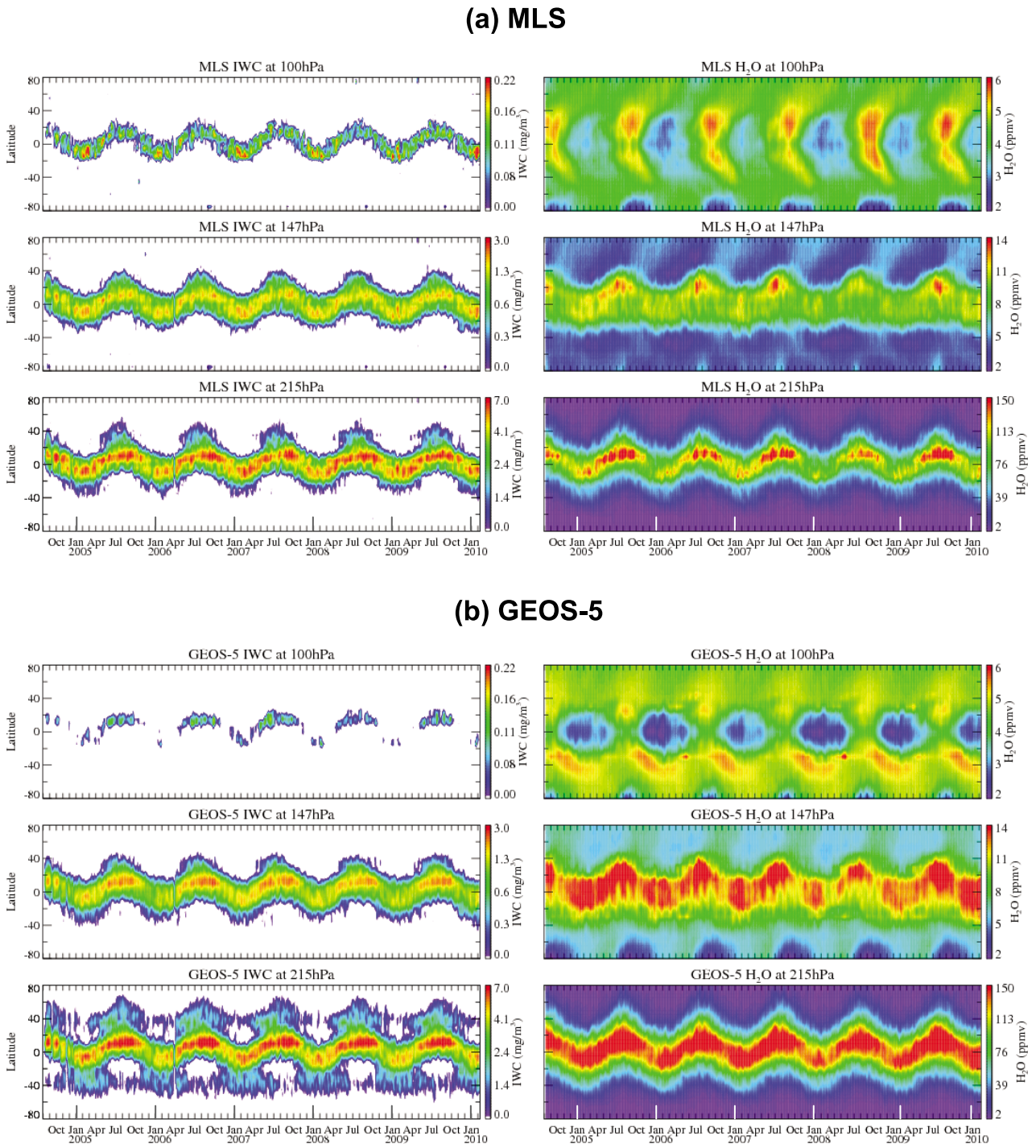

Figure 5. Latitude-time sections of daily zonal-mean IWC and H_2O at 100, 147 and 215 hPa from (a) MLS observations and (b) GEOS-5 analyses, computed from daily zonal mean data (8 August 2004 to 10 February 2010) and smoothed by the Kalman filter.

annual time scales, El Niño-Southern Oscillation (ENSO) related signals dominate the variability. The El Niño (warm phase) patterns at 215 hPa (Figure 7b) are characterized by an enhancement of IWC and H_2O in the central Pacific accompanied by a reduction of IWC and H_2O in the western Pacific from late 2004 to early 2005, late 2006 to early 2007, and late 2009 to early 2010. The opposite patterns are seen during the cold La Niña phase from late 2007 through 2008 and early 2009. IWC anomalies at 100 hPa (Figure 7a) appear in phase with those at 215 hPa, but the H_2O anomalies at 100 hPa are of different characteristics with the 215 hPa IWC and H_2O: they are widespread in longitude,

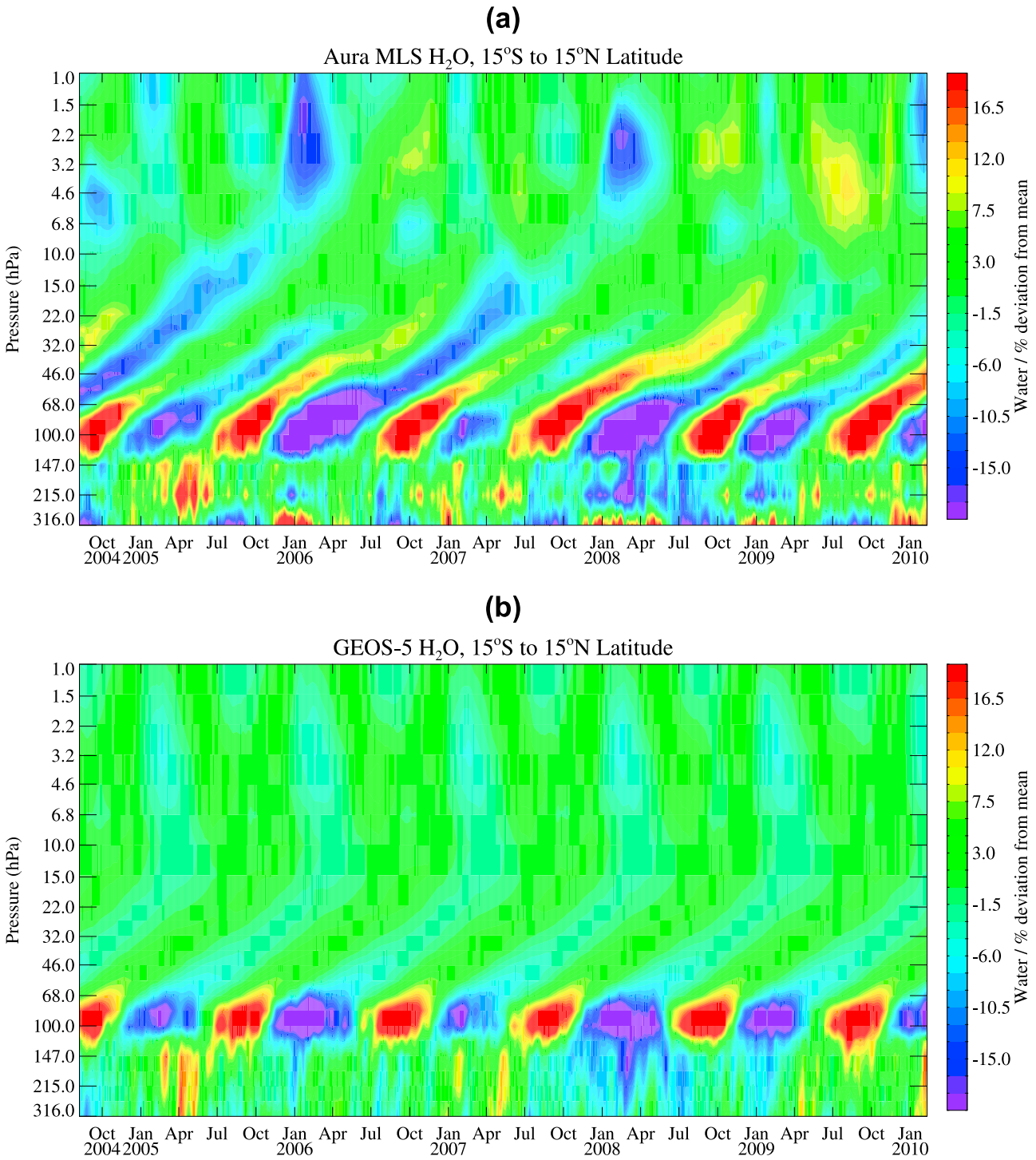

Figure 6. Height-time section of tropical (15°S–15°N) mean daily H_2O anomalies from (a) MLS and (b) GEOS-5. The anomalies are relative to tropical mean averaged from 8 August 2004 to 10 February 2010 time period and smoothed by the Kalman filter. MLS H_2O vertical averaging kernels are not applied to GEOS-5 H_2O in this plot.

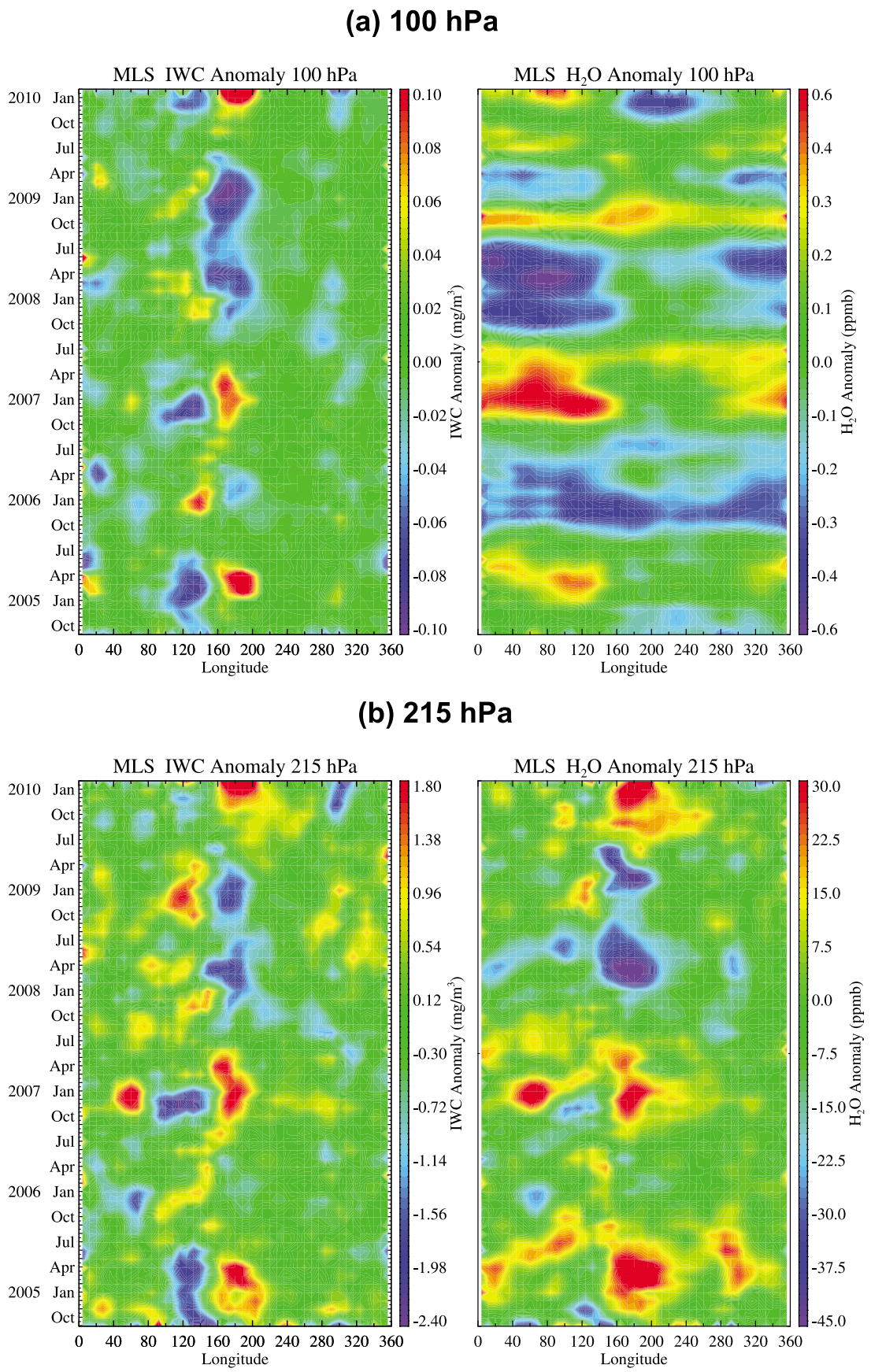

Figure 7. Longitude-time section of tropical (15°S–15°N) mean monthly MLS IWC and H_2O anomalies at (a) 100 hPa and (b) 215 hPa, computed from monthly mean data (September 2004 to January 2010).

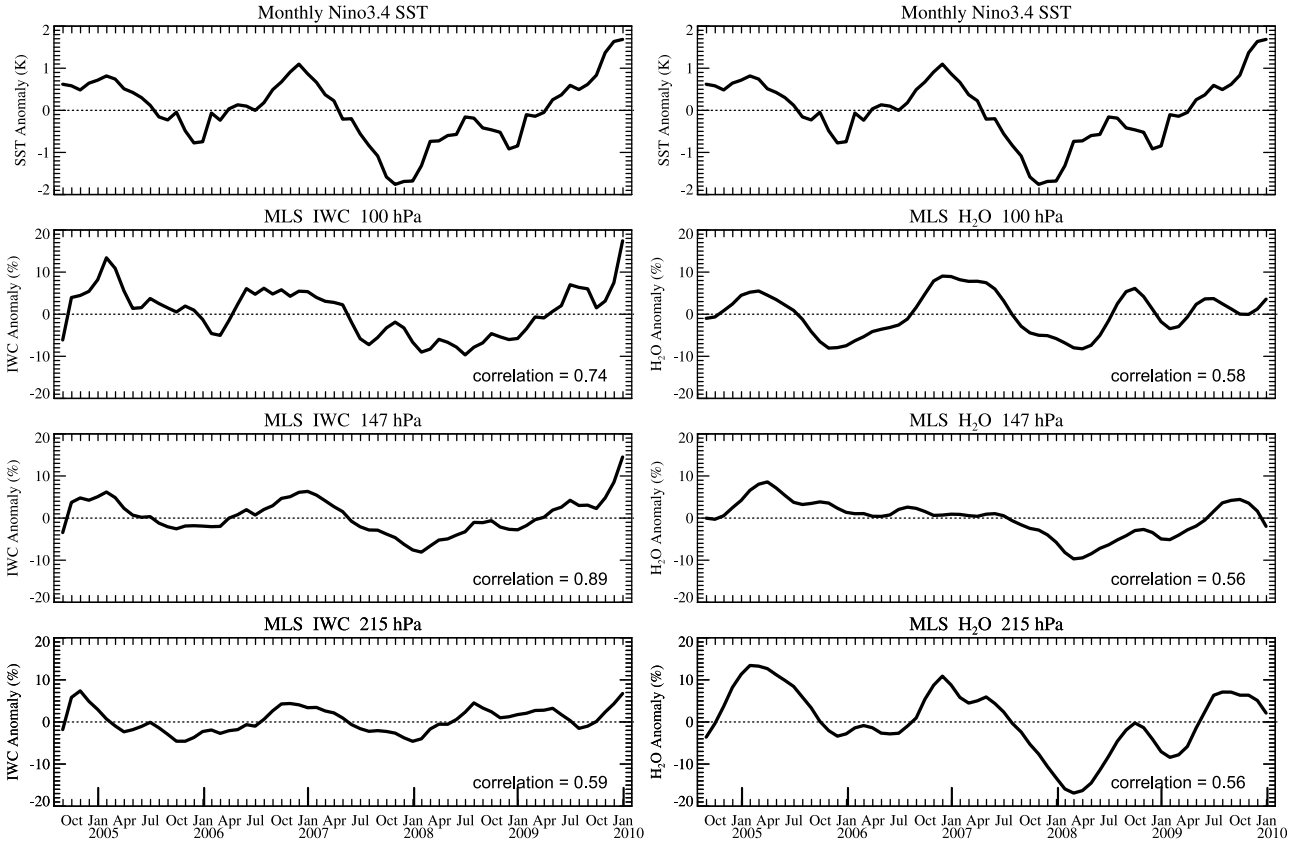

Figure 8. (top to bottom) September 2004 to January 2010 time series of monthly SST anomaly in the Niño 3.4 region (170°–240°, 5°S–5°N) (repeated once), and monthly tropical (15°S–15°N) (left) MLS IWC and (right) H_2O at 100, 147, and 215 hPa. The anomalies are relative to the five-year (2005–2009) climatological monthly means, with a 3-point running smooth applied.

and are strong over the Indian Ocean (also see Figure 9 in section 5). GEOS-5 IWC and H_2O data (see auxiliary material Figure S2) show a similar pattern, except that the 100 hPa IWC is generally weaker in magnitude. For the 2009–2010 winter El Niño event, a strong negative H_2O anomaly is shown in the central-eastern Pacific, unlike the previous two events in 2004–2005 and 2006–2007 winters. The mechanisms for the ENSO anomalies will be investigated in a future study.

5. UT Response to ENSO

[27] The MLS simultaneous and collocated measurements of H_2O, IWC and T provide an unprecedented characterization of the UT response to ENSO. Figure 8 shows time series of monthly Niño 3.4 SST (the SST averaged for longitudes 170°–240° and latitudes 5°S–5°N [see *Trenberth*, 1997]) anomaly, and the monthly tropical (15°S to 15°N) MLS IWC and H_2O anomalies at 100, 147, and 215 hPa (expressed in percentage changes, relative to the 5-year monthly means). The time series of tropical-mean IWC and H_2O anomalies at all three levels have roughly similar time evolution to that of the Niño 3.4 SST. They are positively correlated with the Nino3.4 SST, with correlation coefficients between 0.5 and 0.9. The tropical-mean 100 hPa H_2O anomaly evolution closely follows the 100 hPa temperature anomaly (not shown), which is also positively correlated with the Nino3.4 SST. However, the 100 hPa anomaly patterns are of opposite sign to their counterparts at the lower levels, calling for a further study of the mechanisms that drive the UT temperature and water vapor responses (see Figure 7 and below).

[28] We choose DJF 2005 and 2008 to represent, respectively, the warm and cold phases of ENSO. Figures 9a and 9b show the corresponding IWC, H_2O and T anomalies for the two phases. A typical dipole pattern [*Semazzi and Indeje*, 1999] is seen in IWC and H_2O at 215 and 147 hPa, with positive anomaly in the central Pacific and negative anomaly in the western Pacific during El Niño and the opposite pattern during La Niña. The negative IWC anomaly over the western Pacific during El Niño is an indication of reduced convection in response to warmer SST in the central Pacific [*Su and Neelin*, 2002]. This is possibly associated with anticyclones west of the localized SST heating, as suggested by *Highwood and Hoskins* [1998]. The T anomalies at 215 and 147 hPa are typical of "Gill-type" wave response (a large-scale circulation pattern in response to localized heating, which consists of a Kelvin wave to the east of the heating and a Rossby wave to the west) to a localized heating source and exhibit a more homogenous response than that of IWC and H_2O within the tropics [*Gill*, 1980]. At 100 hPa in DJF 2005, a positive IWC anomaly

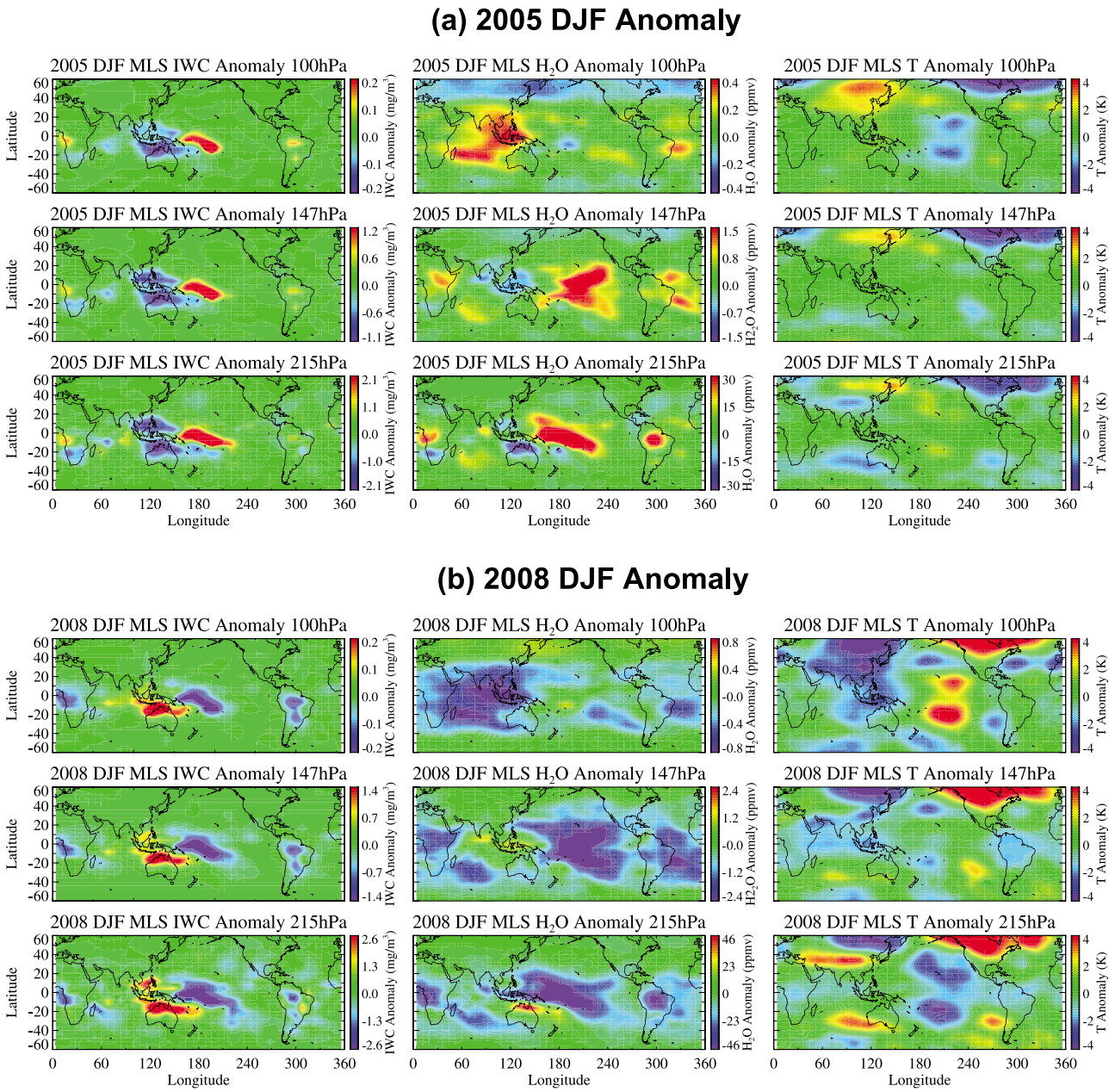

Figure 9. Maps of (a) 2005 DJF and (b) 2008 DJF anomalies of IWC, H_2O and T from MLS measurements. The anomalies are computed as the difference between 2005 or 2008 DJF averages and the five-year seasonal average. Note that the 2005 DJF covers three months from December 2004 to February 2005, while the 2008 DJF refers to December 2007 to February 2008 period. All anomaly maps are computed in 8° longitude × 4° latitude grid boxes.

and a negative H_2O anomaly in the central Pacific are accompanied by anomalies of opposite sign in the western Pacific and the Indian Ocean, with larger amplitude in the Indian Ocean. The 100 hPa H_2O anomaly pattern does not closely resemble that of 100 hPa T. Whether the strong H_2O anomalies over the Indian Ocean represent a teleconnection through "atmospheric bridge" [*Alexander et al.*, 2002; *Klein et al.*, 1999] or a response to local SST anomaly or other dynamics is not clear. A very similar spatial pattern to Figure 9a is obtained (auxiliary material Figure S5) by regressing the MLS UT anomalies onto the Nino3.4 SST, indicating these UT anomalies are primarily driven by ENSO. Opposite-signed anomalies are evident in DJF 2008, a La Niña event. The ENSO response in GEOS-5 (see auxiliary material Figures S3 and S4) is similar to that of MLS.

6. Summary and Conclusions

[29] We have presented Aura MLS UT H_2O, IWC and T measurements made from August 2004 to February 2010, with comparisons to GEOS-5 analyses of these quantities

for the same period. The global distributions of five-year-mean annual and seasonal averages, and tropical temporal evolution and response to ENSO, are given. Comparisons between MLS and GEOS-5 UT temperatures are also discussed.

[30] Agreement between MLS and GEOS-5 H_2O at 100 and 147 hPa is generally within the estimated MLS measurement accuracy of ~20% (albeit slightly worse at 147 hPa, but probably not significant, 30%, comparing to the MLS measurement accuracy). GEOS-5 has (during all seasons) smaller minimum tropical 100 hPa H_2O values and moister extra-tropics than MLS, thought to be caused by the model's relaxation to fixed stratospheric H_2O concentrations. GEOS-5 215 hPa H_2O is larger than MLS values by ~50%, probably because of higher GEOS-5 temperature at this altitude. IWC agreement is within the estimated factor-of-two accuracy of MLS, but comparisons of IWC vertical distributions suggest that GEOS-5 deep convection does not extend sufficiently high. There appears to be a significant difference in 215 hPa temperature, with GEOS-5 being ~1 K warmer after accounting for the known ~2 K cold bias in MLS. MLS and GEOS-5 147 and 100 hPa temperatures agree on average to within ~0.5 K, well within the MLS uncertainty.

[31] The tropical distributions of 215 hPa H_2O and IWC are positively correlated; large values of both are associated with regions of deep convection, as previously found [e.g., *Su et al.*, 2006a]. The distributions of 100 hPa H_2O and IWC are negatively correlated, with less H_2O and more IWC in regions of deep convection, as expected from "freeze-drying" of uplifted air. The transition from positive to negative correlation occurs between 147 and 100 hPa. The tropical 215 hPa H_2O and IWC seasonal variations track regions of deep convection, while the 100 hPa H_2O seasonal variations follow 100 hPa temperature. The largest values of tropical H_2O occur in the northern summer over the South Asia monsoon region; the smallest values of H_2O occur in the northern winter over the western Pacific.

[32] Tropical zonal mean H_2O and IWC exhibit strong seasonal and interannual variations. MLS data show a clear tropical H_2O "tape-recorder" signal in the TTL and stratosphere. GEOS-5 H_2O appears to ascend slightly faster through the upper tropical tropopause (121 hPa–83 hPa,) than does MLS H_2O, and has a smaller amplitude seasonal cycle in the stratosphere (where moisture is relaxed to zonal-mean values). A future GEOS objective is to implement a more realistic stratospheric moisture module which includes methane oxidation chemistry.

[33] Fluctuations in tropical UT H_2O and IWC are associated with moderate El Niño and La Niña events that occurred during the 5-year period analyzed here. H_2O and IWC tropical mean fractional anomalies were about 10%. The IWC and H_2O deseasonalized 215 hPa anomalies exhibit a dipole pattern during El Niño (La Niña), with positive (negative) anomalies in the eastern Pacific and negative (positive) anomalies in the western Pacific. A strong positive (negative) 100 hPa H_2O anomaly occurs over the Indian Ocean during El Niño (La Niña). The mechanisms responsible for it needs further study.

[34] This paper is an example of using satellite measurements to evaluate global models. We emphasize that it is imperative to ensure consistent spatial and temporal sampling between model outputs and satellite measurements, and application of measurement averaging kernels to modeled vertical profiles, for a fair comparison. In our study, GEOS-5 results are interpolated onto the MLS measurement locations in both space and time, and with MLS averaging kernels applied to produce vertical profiles. Thus, the differences between the model and measurements are mostly due to the model physics, rather than sampling artifacts.

[35] **Acknowledgments.** The authors acknowledge the support from the Aura MLS project, Jet Propulsion Laboratory, California Institute of Technology, conducted under contract with NASA. We also acknowledge the support by NASA's Modeling and Analysis Program (MAP) for the Global Modeling and Assimilation Office at NASA Goddard Space Flight Center. The GEOS-5 data assimilation system is run on NASA's High-Performance Computing (HEC) resources at NASA's Goddard Research Center.

References

Alexander, M. A., I. Blade, M. Newman, J. R. Lanzante, N. C. Lau, and J. D. Scott (2002), The atmospheric bridge: The influence of ENSO teleconnections on air–sea interaction over the global oceans, *J. Clim.*, *15*, 2205–2231, doi:10.1175/1520-0442(2002)015<2205:TABTIO>2.0.CO;2.

Bacmeister, J. T., M. J. Suarez, and F. R. Robertson (2006), Rain re-evaporation, boundary layer–convection interactions, and Pacific rainfall patterns in an AGCM, *J. Atmos. Sci.*, *63*, 3383–3403, doi:10.1175/JAS3791.1.

Baldwin, M. P., et al. (2001), The Quasi-Biennial Oscillation, *Rev. Geophys.*, *39*, 179–229, doi:10.1029/1999RG000073.

Bloom, S., L. Takacs, A. DaSilva, and D. Ledvina (1996), Data assimilation using incremental analysis updates, *Mon. Weather Rev.*, *124*, 1256–1271, doi:10.1175/1520-0493(1996)124<1256:DAUIAU>2.0.CO;2.

Corti, T., B. P. Luo, Q. Fu, H. Vömel, and T. Peter (2006), The impact of cirrus clouds on tropical troposphere-to-stratosphere transport, *Atmos. Chem. Phys.*, *6*, 2539–2547, doi:10.5194/acp-6-2539-2006.

Danielsen, E. F. (1968), Stratospheric-tropospheric exchange based on radioactivity, ozone and potential vorticity, *J. Atmos. Sci.*, *25*, 502–518, doi:10.1175/1520-0469(1968)025<0502:STEBOR>2.0.CO;2.

Fetzer, E. J., et al. (2008), Comparison of upper tropospheric water vapor observations from the Microwave Limb Sounder and Atmospheric Infrared Sounder, *J. Geophys. Res.*, *113*, D22110, doi:10.1029/2008JD010000.

Fu, R., Y. Hu, J. S. Wright, J. H. Jiang, R. E. Dickinson, M. Chen, M. Filipiak, W. G. Read, J. W. Waters, and D. L. Wu (2006), Short circuit of water vapor and polluted air to the global stratosphere by convective transport over the Tibetan Plateau, *Proc. Natl. Acad. Sci. U. S. A.*, *103*, 5664–5669, doi:10.1073/pnas.0601584103.

Gill, A. (1980), Some simple solutions for heat-induced tropical circulations, *Q. J. R. Meteorol. Soc.*, *106*, 447–462, doi:10.1002/qj.49710644905.

Hartmann, D. L., and M. L. Michelsen (2002), No evidence for iris, *Bull. Am. Meteorol. Soc.*, *83*, 249–254, doi:10.1175/1520-0477(2002)083<0249:NEFI>2.3.CO;2.

Hartmann, D. L., J. R. Holton, and Q. Fu (2001), The heat balance of the tropical tropopause, cirrus, and stratospheric dehydration, *Geophys. Res. Lett.*, *28*, 1969–1972, doi:10.1029/2000GL012833.

Held, I. H., and B. J. Soden (2000), Water vapor feedback and global warming, *Annu. Rev. Energy Environ.*, *25*, 441–475, doi:10.1146/annurev.energy.25.1.441.

Highwood, E. J., and B. J. Hoskins (1998), The tropical tropopause, *Q. J. R. Meteorol. Soc.*, *124*, 1579–1604, doi:10.1002/qj.49712454911.

Highwood, E. J., B. J. Hoskins, and P. Berrisford (2000), Properties of the arctic tropopause, *Q. J. R. Meteorol. Soc.*, *126*, 1515–1532, doi:10.1256/smsqj.56514.

Holton, J. R., and A. Gettelman (2001), Horizontal transport and the dehydration of the stratosphere, *Geophys. Res. Lett.*, *28*, 2799–2802, doi:10.1029/2001GL013148.

Klein, S. A., B. J. Soden, and N.-C. Lau (1999), Remote sea surface variations during ENSO: Evidence for a tropical atmospheric bridge, *J. Clim.*, *12*, 917–932, doi:10.1175/1520-0442(1999)012<0917:RSSTVD>2.0.CO;2.

Li, J.-L., et al. (2005), Comparisons of EOS MLS cloud ice measurements with ECMWF analyses and GCM simulations: Initial results, *Geophys. Res. Lett.*, *32*, L18710, doi:10.1029/2005GL023788.

Li, J.-L., J. H. Jiang, D. E. Waliser, and A. M. Tompkins (2007), Assessing Consistency between EOS MLS and ECMWF analyzed and forecast estimates of cloud ice, *Geophys. Res. Lett.*, *34*, L08701, doi:10.1029/2006GL029022.

Lin, B., B. Wielicki, L. Chambers, Y. Hu, and K.-M. Xu (2002), The iris hypothesis: A negative or positive cloud feedback?, *J. Clim.*, *15*, 3–7, doi:10.1175/1520-0442(2002)015<0003:TIHANO>2.0.CO;2.

Lin, S.-J. (2004), A vertically Lagrangian finite-volume dynamical core for global models, *Mon. Weather Rev.*, *132*, 2293–2307, doi:10.1175/1520-0493(2004)132<2293:AVLFDC>2.0.CO;2.

Lindzen, R. S., M.-D. Chou, and A. Y. Hou (2001), Does the Earth have an adaptive infrared iris?, *Bull. Am. Meteorol. Soc.*, *82*, 417–432, doi:10.1175/1520-0477(2001)082<0417:DTEHAA>2.3.CO;2.

Livesey, N. J., W. V. Snyder, W. G. Read, and P. A. Wagner (2006), Retrieval algorithms for the EOS Microwave Limb Sounder (MLS) instrument, *IEEE Trans. Geosci. Remote Sens.*, *44*, 1144–1155, doi:10.1109/TGRS.2006.872327.

Livesey, N. J., et al. (2007), EOS MLS version 2.2 Level 2 data quality and description document, *Tech. Rep. JPL D-33509*, Jet Propul. Lab, Pasadena, Calif.

Moorthi, S., and M. J. Suarez (1992), Relaxed Arakawa-Schubert—A parameterization of moist convection for general-circulation models, *Mon. Weather Rev.*, *120*, 978–1002, doi:10.1175/1520-0493(1992)120<0978:RASAPO>2.0.CO;2.

Mote, P. W., K. H. Rosenlof, M. E. McIntyre, E. S. Carr, J. R. Holton, J. S. Kinnersley, H. C. Pumphrey, J. M. Russell III, J. W. Waters, and J. C. Gille (1996), An atmospheric tape recorder: the imprint of tropical tropopause temperatures on stratospheric water vapor, *J. Geophys. Res.*, *101*(D2), 3989–4006, doi:10.1029/95JD03422.

Park, M., W. J. Randel, A. Gettleman, S. T. Massie, and J. H. Jiang (2007), Transport above the Asian summer monsoon anticyclone inferred from Aura MLS tracers, *J. Geophys. Res.*, *112*, D16309, doi:10.1029/2006JD008294.

Read, W. G., D. L. Wu, J. W. Waters, and H. C. Pumphrey (2004), Dehydration in the tropical tropopause layer: Implications from the UARS Microwave Limb Sounder, *J. Geophys. Res.*, *109*, D06110, doi:10.1029/2003JD004056.

Read, W. G., et al. (2007), Aura Microwave Limb Sounder upper tropospheric and lower stratospheric H_2O and relative humidity with respect to ice validation, *J. Geophys. Res.*, *112*, D24S35, doi:10.1029/2007JD008752.

Read, W. G., M. J. Schwartz, A. Lambert, H. Su, N. J. Livesey, W. H. Daffer, and C. D. Boone (2008), The roles of convection, extratropical mixing, and in situ freeze-drying in the tropical tropopause layer, *Atmos. Chem. Phys.*, *8*, 6051–6067, doi:10.5194/acp-8-6051-2008.

Rienecker, M. M., et al. (2008), The GEOS-5 data assimilation system—Documentation of versions 5.0.1, 5.1.0, and 5.2.0, *NASA Tech. Memo., TM–2008–104606*, vol. 27, 97 pp.

Sasaki, Y. (1970), Some basic formalisms in numerical variational analysis, *Mon. Weather Rev.*, *98*, 875–883, doi:10.1175/1520-0493(1970)098<0875:SBFINV>2.3.CO;2.

Schoeberl, M. R. (2004), Extra-tropical stratosphere-troposphere mass exchange, *J. Geophys. Res.*, *109*, D13303, doi:10.1029/2004JD004525.

Schwartz, M. J., et al. (2008), Validation of the Aura Microwave Limb Sounder temperature and geopotential height measurements, *J. Geophys. Res.*, *113*, D15S11, doi:10.1029/2007JD008783.

Semazzi, F. H. M., and M. Indeje (1999), Inter-seasonal variability of ENSO rainfall signal over Africa, *J. Afr. Meteorol. Soc.*, *4*, 81–94.

Sherwood, S. C., and A. E. Dessler (2001), A model for transport across the tropical tropopause, *J. Atmos. Sci.*, *58*, 765–779, doi:10.1175/1520-0469(2001)058<0765:AMFTAT>2.0.CO;2.

Soden, B. J., and R. Fu (1995), A satellite analysis of deep convection, upper-tropospheric humidity, and the greenhouse effect, *J. Clim.*, *8*, 2333–2351, doi:10.1175/1520-0442(1995)008<2333:ASAODC>2.0.CO;2.

Soden, B. J., D. L. Jackson, V. Ramaswamy, M. D. Schwarzkopf, and X. Huang (2005), The radiative signature of upper tropospheric moistening, *Science*, *310*(5749), 841–844, doi:10.1126/science.1115602.

Stephens, G. L. (1990), On the relationship between water vapor over the oceans and sea surface temperature, *J. Clim.*, *3*, 634–645.

Su, H., and J. D. Neelin (2002), Teleconnection mechanisms for tropical Pacific descent anomalies during El Nino, *J. Atmos. Sci.*, *59*, 2694–2712, doi:10.1175/1520-0469(2002)059<2694:TMFTPD>2.0.CO;2.

Su, H., W. G. Read, J. H. Jiang, J. W. Waters, D. L. Wu, and E. J. Fetzer (2006a), Enhanced positive water vapor feedback associated with tropical deep convection: New evidence from Aura MLS, *Geophys. Res. Lett.*, *33*, L05709, doi:10.1029/2005GL025505.

Su, H., D. E. Waliser, J. H. Jiang, J.-L. Li, W. G. Read, J. W. Waters, and A. M. Tompkins (2006b), Relationships of upper tropospheric water vapor, clouds and SST: MLS observations, ECMWF analyses and GCM simulations, *Geophys. Res. Lett.*, *33*, L22802, doi:10.1029/2006GL027582.

Su, H., J. H. Jiang, G. L. Stephens, D. G. Vane, and N. J. Livesey (2009), Radiative effects of upper tropospheric clouds observed by Aura MLS and CloudSat, *Geophys. Res. Lett.*, *36*, L09815, doi:10.1029/2009GL037173.

Sud, Y., and G. K. Walker (1999), Microphysics of Clouds with the Relaxed Arakawa Schubert Scheme (McRAS). Part I: Design and evaluation with GATE Phase III data, *J. Atmos. Sci.*, *56*, 3196–3220, doi:10.1175/1520-0469(1999)056<3196:MOCWTR>2.0.CO;2.

Trenberth, K. E. (1997), The definition of El Niño, *Bull. Am. Meteorol. Soc.*, *78*, 2771–2777, doi:10.1175/1520-0477(1997)078<2771:TDOENO>2.0.CO;2.

Udelhofen, P. M., and D. L. Hartmann (1995), Influence of tropical cloud systems on the relative humidity in the upper troposphere, *J. Geophys. Res.*, *100*, 7423–7440, doi:10.1029/94JD02826.

Waliser, D. E., et al. (2009), Cloud ice: A climate model challenge with signs and expectations of progress, *J. Geophys. Res.*, *114*, D00A21, doi:10.1029/2008JD010015.

Waters, J. W., et al. (2006), The Earth Observing System Microwave Limb Sounder (EOS MLS) on the Aura satellite, *IEEE Trans. Geosci. Remote Sens.*, *44*, 1075–1092, doi:10.1109/TGRS.2006.873771.

Wu, D. L., and J. H. Jiang (2004), EOS MLS algorithm theoretical basis for cloud measurements, *Tech. Rep. JPL D-19299*, Jet Propul. Lab., Pasadena, Calif.

Wu, D. L., J. H. Jiang, W. G. Read, R. T. Austin, C. P. Davis, A. Lambert, G. L. Stephens, D. G. Vane, and J. W. Waters (2008), Validation of the Aura MLS cloud ice water content measurements, *J. Geophys. Res.*, *113*, D15S10, doi:10.1029/2007JD008931.

Wu, W.-S., R. J. Purser, and D. F. Parrish (2002), Three-dimensional variational analysis with spatially inhomogeneous covariances, *Mon. Weather Rev.*, *130*, 2905–2916, doi:10.1175/1520-0493(2002)130<2905:TDVAWS>2.0.CO;2.

R. A. Fuller, J. H. Jiang, A. Lambert, J. N. Lee, N. J. Livesey, W. G. Read, M. L. Santee, M. J. Schwartz, H. Su, J. W. Waters, and D. L. Wu, Jet Propulsion Laboratory, California Institute of Technology, MS 183-701, 4800 Oak Grove Dr., Pasadena, CA 91109-8099, USA. (jonathan.h.jiang@jpl.nasa.gov)

H.-C. Liu and S. Pawson, Global Modeling and Assimilation Office, NASA Goddard Space Flight Center, Greenbelt, MD 20771-0001, USA.